Catalysis Today 157 (2010) 415–419

Contents lists available at ScienceDirect

Catalysis Today

journal homepage: www.elsevier.com/locate/cattod

# Activation of $Pt/SnO_2$ catalyst for catalytic oxidation of volatile organic compounds

Naoto Kamiuchi, Tomohiro Mitsui, Nobutada Yamaguchi, Hiroki Muroyama, Toshiaki Matsui, Ryuji Kikuchi[1], Koichi Eguchi*

*Department of Energy and Hydrocarbon Chemistry, Graduate School of Engineering, Kyoto University, Nishikyo-ku, Kyoto 615-8510, Japan*

ARTICLE INFO

*Article history:*
Available online 3 April 2010

*Keywords:*
Platinum
Ruthenium
Palladium
Rhodium
Tin oxide
Catalyst
Catalytic combustion
Structural change
Chemical interaction
TEM

ABSTRACT

The catalytic combustion of toluene over tin oxide-supported metal catalysts ($Pt/SnO_2$, $Pd/SnO_2$, $Ru/SnO_2$, and $Rh/SnO_2$) was studied. As a result, the $Pt/SnO_2$ catalyst exhibited the highest activity. The activity of $Pt/SnO_2$ catalyst is expected to originate from the strong chemical interaction between platinum and tin oxide. The correlation between the nano-structure and catalytic activity in the oxidation of ethyl acetate was investigated for the $Pt/SnO_2$ catalysts treated under a reducing or an oxidative atmosphere. For the transmission electron microscopy image of the as-calcined $Pt/SnO_2$ catalyst, the fine particles composed of platinum species was highly dispersed on the surface of $SnO_2$ support. After the reduction treatment at 400 °C, the peculiar core–shell structure was formed. It is noted that the particles with this structure disappeared by the reoxidation treatment in air, and the redispersion of nano-particles was confirmed. The particles with the core–shell structure were observed again after the second reduction treatment for the reoxidized catalyst. The catalytic activities of ethyl acetate combustion over $Pt/SnO_2$ catalysts were deteriorated and activated, corresponding to the nano-structural changes induced by the reduction–oxidation treatments.



## 1. Introduction

The emission of volatile organic compounds (VOCs) such as ethyl acetate, toluene, acetaldehyde, has been recognized as a critical problem. This is because these compounds cause the acid rain and photochemical smog by the photochemical reaction with $NO_x$ [1–4]. They are also known as the causative substances of the sick house syndrome. Therefore, the decomposition techniques of VOCs have been investigated so far. The combustion at low temperatures by the supported precious metal catalysts is one of the most effective methods for the abatement of VOCs [5–7]. For instance, the complete oxidation of acetic acid was achieved below 400 °C by using $Pd/\gamma\text{-}Al_2O_3$ catalyst, whereas the combustion over $\gamma\text{-}Al_2O_3$ proceeded insufficiently even at 600 °C [8].

The catalytic activities of the precious metal catalysts are strongly affected by many factors such as the kinds of precious metal and metal oxide support, their combination, the pretreatment condition, the precious metal source, the preparation method, and so on. Furthermore, the strong chemical interaction between precious metal and metal oxide support often influences the catalytic property. Thereby, to design the supported precious metal catalyst with high activity often encounters difficulties. In particular, the $SnO_2$-supported precious metal catalysts have the peculiar property due to the strong chemical interaction between the precious metal and $SnO_2$ support. The catalyst of $Pd/SnO_2$ [9–12] and $Ru/SnO_2$ [13] exhibited the high catalytic activities for the methane combustion and ethyl acetate combustion, respectively, in spite of the low surface area. The $Pt/SnO_2$ catalyst reduced in hydrogen is active for the electrochemical CO oxidation, and is the prospective materials for the electrode catalyst of the polymer electrolyte fuel cells (PEFCs) [14–16].

In this report, toluene and ethyl acetate, which are typical volatile organic compounds, were used for the catalytic combustion test. The catalytic activities over the precious metal catalysts supported on $SnO_2$ were evaluated together with their surface area, XPS, and TEM analysis. The notable phenomena such as the high dispersion of the precious metal species, the formation of core–shell structure, and the redispersion of the precious metal particles were observed in $Pt/SnO_2$ [17,18] and $Ru/SnO_2$ [19]. Then, the correlation between the nano-structure and catalytic activity of $Pt/SnO_2$ catalyst, which showed the highest activity in toluene combustion, was closely investigated.

* Corresponding author. Tel.: +81 75 383 2519; fax: +81 75 383 2520.
*E-mail address:* eguchi@scl.kyoto-u.ac.jp (K. Eguchi).
[1] Present address: Department of Chemical System Engineering, The University of Tokyo, 7-3-1 Hongo, Bunkyo-ku, Tokyo 113-8656, Japan.

0920-5861/$ – see front matter © 2010 Elsevier B.V. All rights reserved.
doi:10.1016/j.cattod.2010.02.063

**Table 1**
Heat-treatment of $Pt/SnO_2$ catalysts.

| Sample name | Heat-treatment |
|---|---|
| S-1 | As-calcined |
| S-2 | Reduction[a] at 400 °C for 0.5 h |
| S-3 | Reduction at 400 °C for 0.5 h, followed by reoxidation[b] at 400 °C for 0.5 h |
| S-4 | Reoxidation at 400 °C for 0.5 h, followed by second reduction[b] at 400 °C for 0.5 h |

[a] Reduction atmosphere: 10% $H_2/N_2$.
[b] Oxidation atmosphere: air.

## 2. Experimental

### 2.1. Catalyst preparation

The $SnO_2$-supported precious metal catalysts ($Pt/SnO_2$, $Pd/SnO_2$, $Ru/SnO_2$, and $Rh/SnO_2$) were prepared by the impregnation method. Solutions of $Pt(NO_2)_2(NH_3)_2$, $Pd(NO_2)_2(NH_3)_2$, $Ru(NO_3)_3$, or $Rh(NO_3)_3$ (Tanaka Kikinzoku Kogyo) were used as metal sources. The powder of tin oxide (Wako Pure Chemical Industries Ltd.) calcined at 800 °C for 5 h in air was applied as a support. The tin oxide powder was impregnated with the solution containing the precious metal. The mixture was kept on a steam bath at 80 °C to evaporate sufficiently. The resulting powder was calcined at 400 °C for 0.5 h in air. A part of $Pt/SnO_2$ catalyst calcined at 400 °C (S-1) was heat-treated under the reduction–oxidation conditions summarized in Table 1. The metal loading amount in the catalysts was fixed at 1.0 and 10 wt.%. In the catalytic combustion test, the 1.0 wt.% catalysts were used. The analyses of 1.0 wt.% catalysts by the X-ray apparatuses were hard due to the low loading amount of precious metal. Thus, the catalysts with heavy loading amount were prepared to investigate the surface electronic states and the crystal phases by the X-ray apparatuses, though the 10 wt.% catalysts are impractical. The loading amount of precious metal may affect the catalytic properties, while it was verified that the properties of 1.0 wt.% $Pt/SnO_2$ was essentially the same as those of 20 wt.% $Pt/SnO_2$ [17,18].

### 2.2. Catalytic combustion of toluene and ethyl acetate

A fixed-bed flow reactor made of quartz tubing with 8 mm inner diameter was used, and the as-calcined catalyst (600 mg) was set in the reactor. All catalysts with 1.0 wt.% Pt, Pd, Ru, and Rh were tableted and pulverized into 10–26 mesh before catalytic reaction tests. In the case of toluene and ethyl acetate combustions, gaseous mixtures composed of 1.0% toluene–99% air and 0.1% ethyl acetate–99.9% air were fed with a flow rate of 100 ml $min^{-1}$, respectively (space velocity: 10,000 l $kg^{-1}$ $h^{-1}$). The outlet gas compositions were analyzed by an on-line gas chromatograph with a thermal conductivity detector (TCD) (VARIAN, CP-4900) and a flame ionization detector (FID) (Shimadzu, GC-8A). The conversion was calculated based on $CO_2$ concentration at the reactor outlet. The temperature was raised from room temperature up to 350 °C at a heating rate of 100 °C $h^{-1}$. The catalytic reaction tests were started after the concentration of toluene or ethyl acetate and $CO_2$ in the outlet gas became constant.

### 2.3. Characterization by BET, XRD, XPS, and FE-TEM

The prepared precious metal catalysts were carefully characterized by X-ray photoelectron spectroscopy (XPS), BET surface area, X-ray diffraction (XRD), and transmission electron microscopy (TEM). The XPS (Shimadzu ESCA-3400 and ESCA-850, Mg Kα radiation) measurements were carried out in order to analyze the surface electronic state and atomic ratio (precious metal/Sn). The all binding energies were referred to the C 1s peak (285.0 eV). The surface atomic ratios were calculated from the peak area of precious metal and Sn 3d spectra. The BET surface area was determined by $N_2$ adsorption at the liquid nitrogen temperature using a BEL Japan Bellsorp-mini II analyzer. The phase identification of the samples was conducted by XRD with Cu Kα radiation (Rigaku Rint 1400 X-ray diffractometer). The morphologies of the catalysts were observed by FE-TEM (Philips CM200 FEG) which was equipped with a field emission electron gun, a CCD camera and digital micrograph software (Gatan). The mean particle diameter was obtained by the analysis of the images obtained by TEM (Hitachi H-9000). For the specimens for TEM observation, the catalysts were dispersed in ethanol solution by ultrasonic wave, and the resulting solution was dropped on carbon coated copper microgrids (Oken-shoji Co., Ltd.).

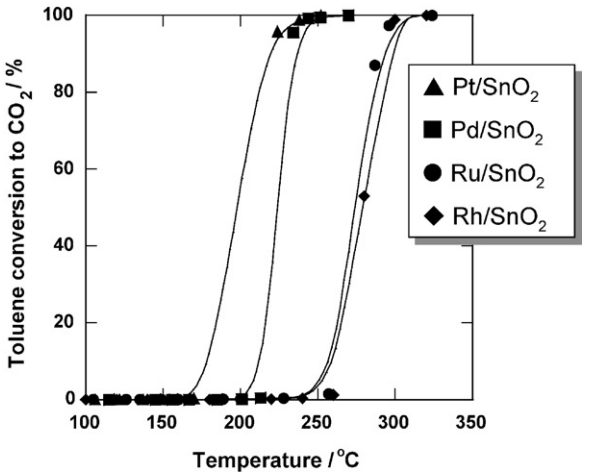


**Fig. 1.** Toluene conversion as a function of temperature over $SnO_2$-supported metal catalysts. Reaction conditions: toluene, 1%; air, 99%; S.V. = 10,000 l $kg^{-1}$ $h^{-1}$; heating rate, 100 °C $h^{-1}$.

## 3. Results and discussion

### 3.1. Toluene combustion over the supported precious metal catalysts

The results of the toluene combustion over the as-calcined 1.0 wt.% $Pt/SnO_2$, $Pd/SnO_2$, $Ru/SnO_2$, and $Rh/SnO_2$ are shown in Fig. 1. Among the catalysts, the $Pt/SnO_2$ catalyst exhibited the highest activity and the lowest ignition temperature of *ca.* 170 °C. The high catalytic activity was also achieved on the $Pd/SnO_2$ catalyst. Although the ignition temperature for the $Pd/SnO_2$ catalyst was *ca.* 200 °C, the temperature of complete oxidation was comparable to that for $Pt/SnO_2$. The catalytic activities of $Ru/SnO_2$ and $Rh/SnO_2$ were lower than those of $Pt/SnO_2$ and $Pd/SnO_2$.

The XRD analyses, BET surface area measurements, and XPS measurements were carried out for all catalysts in order to elucidate the difference in the catalytic activities. The phases ascribed to the precious metal species were not detected by the XRD analysis even in the catalysts with the loading amount of 10 wt.%, whereas the $SnO_2$ phase was clearly observed for all samples. This indicates that the deposits of precious metal species were in the amorphous state or in the highly dispersed state with the extremely small size. The BET surface areas and the results of XPS measurements for 1.0 wt.% catalysts were summarized in Table 2. The surface areas of all catalysts were around 5 $m^2$ $g^{-1}$. As the results of XPS measurements, the peak position of Pt 4f, Pd 3d, Ru 3d, and Rh 3d spectra were located at 75.0, 337.1, 280.8, and 309.6 eV, respectively. The binding energies of Pd 3d, Ru 3d, and Rh 3d agreed well with the reported value of Pd(II) 337.0 eV, Ru(II) 280.7 eV, and Rh(III)

**Table 2**
Surface area, binding energy and surface atomic ratio of the 1.0 wt.% precious metal catalysts calcined at 400 °C.

| Catalyst | BET surface area ($m^2\ g^{-1}$) | Binding energy (eV) | | Surface atomic ratio (M/Sn) |
|---|---|---|---|---|
| $Pt/SnO_2$ | 5.6 | Pt $4f_{7/2}$ | 75.0 | 0.075 |
| $Pd/SnO_2$ | 4.8 | Pd $3d_{5/2}$ | 337.1 | 0.058 |
| $Ru/SnO_2$ | 4.5 | Ru $3d_{5/2}$ | 280.8 | 0.015 |
| $Rh/SnO_2$ | 5.3 | Rh $3d_{5/2}$ | 309.6 | 0.13 |

309.4 eV. On the other hand, the binding energy of platinum was the value between Pt(II) (73.9 eV) and Pt(IV) (75.3 eV), indicating that the platinum species on $SnO_2$ support were in the higher oxidation state than that of PtO. The surface atomic ratio on the $Rh/SnO_2$ catalyst (Rh/Sn = 0.13) was quite larger than those on other catalysts. From these results, the catalytic activities of toluene combustion hardly depended on the surface area and the surface atomic ratio of the $SnO_2$-supported catalysts. From the TPR profiles of 1.0 wt.% $Pt/SnO_2$ calcined at 400 °C, it was revealed that the platinum species can be reduced below 100 °C [20]. Thereby, it was concluded that the highest catalytic activity of $Pt/SnO_2$ catalyst originated from the reducibility of the platinum species in the high oxidation state. These catalytic property of $Pt/SnO_2$ should result from the strong chemical interaction between platinum and $SnO_2$.

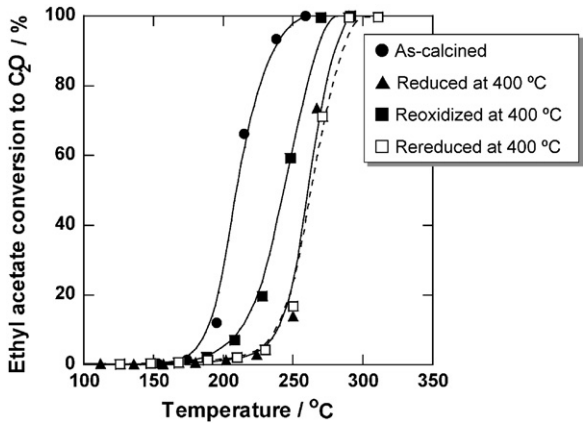


**Fig. 2.** Ethyl acetate conversion as a function of temperature over 1.0 wt.% $Pt/SnO_2$ catalysts. Reaction conditions: ethyl acetate, 0.1%; air, 99.9%; S.V. = 10,000 l $kg^{-1}$ $h^{-1}$; heating rate, 100 °C $h^{-1}$.

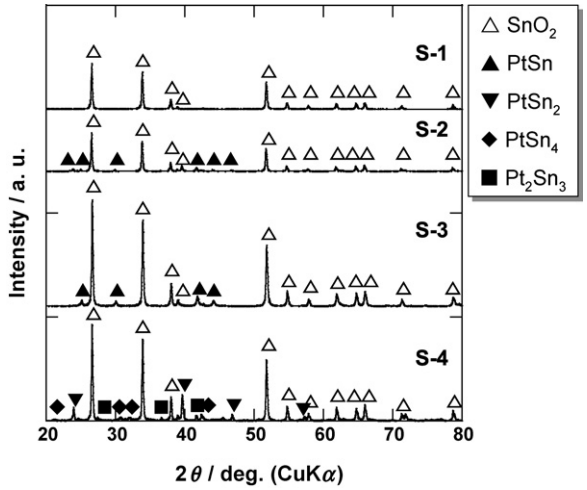


**Fig. 3.** XRD patterns of 10 wt.% $Pt/SnO_2$ catalysts (S-1 ~ S-4).

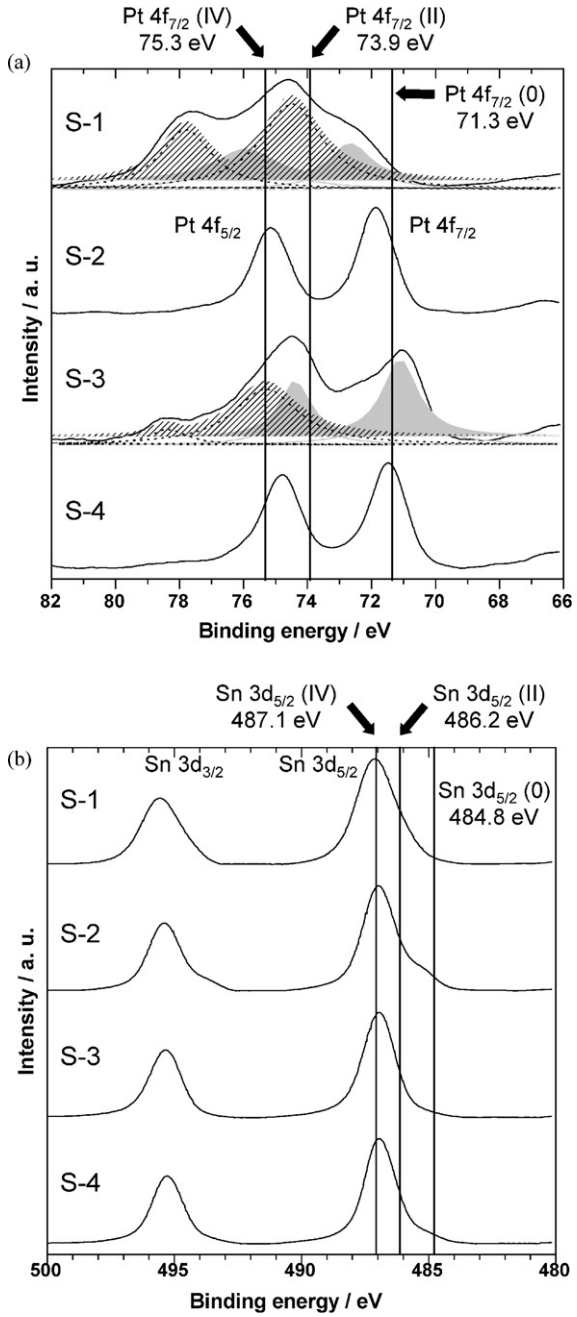


**Fig. 4.** XPS spectra of 10 wt.% $Pt/SnO_2$ catalysts: (a) Pt 4f and (b) Sn 3d.

### *3.2. Catalytic activities of ethyl acetate combustion over $Pt/SnO_2$ catalysts*

The as-calcined $Pt/SnO_2$ catalyst exhibited the high catalytic activity for toluene combustion due to the strong chemical interaction as suggested in the previous section. It is reported that the nano-structure of the $Pt/SnO_2$ catalyst can be easily changed by the heat-treatment due to this strong interaction [17,18]. Then, the relation between the catalytic activities and the morphology of the $Pt/SnO_2$ catalyst subjected to various heat-treatments was investigated.

The catalytic activities of ethyl acetate combustion over 1.0 wt.% $Pt/SnO_2$ catalysts (S-1 ~ S-4) are shown in Fig. 2. In the case of the as-calcined catalyst (S-1), the oxidation of ethyl acetate was started at *ca.* 170 °C, followed by the steep increase up to 100% at 250 °C. The degradation of catalytic activity was induced by the reduction

treatment at 400 °C. The ignition temperature of ethyl acetate over the reduced catalyst was higher than 200 °C. On the other hand, it is of interest that the oxidation reaction of ethyl acetate was initiated at *ca.* 180 °C after the reoxidation treatment at 400 °C. However, the catalytic activity was reversibly deteriorated by the second reduction treatment. The oxidation onset temperature of ethyl acetate over the second reduced catalyst (S-4) was comparable to that over the reduced catalyst (S-2). The variation in catalytic activities depended on the heat-treatment under the reduction–oxidation condition.

The characterizations for the $Pt/SnO_2$ catalysts treated under several conditions were conducted so as to clarify the variation in catalytic activities. The XRD patterns of 10 wt.% $Pt/SnO_2$ catalysts (S-1 ~ S-4) were shown in Fig. 3. As mentioned in the previous section, phases corresponding to platinum species were hardly detected in the as-calcined sample (S-1). In the case of the reduced sample (S-2), the $SnO_2$ and PtSn phases were confirmed. The formation of the intermetallic compound (PtSn) indicated that the platinum species and the surface of $SnO_2$ particles were readily reduced under the heat-treatment at 400 °C in hydrogen. This is supported by the report that the platinum oxide species in 10 wt.% $Pt/SnO_2$ catalyst can be reduced below 100 °C [20]. The $SnO_2$ and PtSn phases were also detected in the reoxidized sample (S-3). The catalytic activity over the reoxidized sample was different from that over the reduced sample, though the same phases were detected by XRD analysis. Thus, the nano-structure in the undetectable level will be significant to the catalytic activity. Meanwhile, the patterns of the intermetallic compound ($PtSn_2$, $PtSn_4$, and $Pt_2Sn_3$) in addition to $SnO_2$ and PtSn were observed by the second reduction treatment. The formation of the intermetallic compound appears to be facilitated by the twice reduction treatments.

The Pt 4f and Sn 3d spectra of 10 wt.% $Pt/SnO_2$ catalysts were measured by XPS as shown in Fig. 4(a) and (b), respectively. The Pt 4f spectra of S-1 and S-3 were deconvoluted to the spectrum corresponding to the gray area and the hatched area. The latter spectrum is attributed to the platinum species in the higher oxidation state than the former spectrum. From the deconvoluted spectra of S-1, it is apparent that the platinum components were in the oxidation state. In contrast, the sharp peaks were located at *ca.* 72.0 eV in the Pt 4f spectra of S-2. Then, the surface electronic state of the platinum particles in the catalyst in S-2 was the metallic one. After the reoxidation treatment, the spectrum of S-3 was separated to the Pt $4f_{7/2}$ spectra around *ca.* 75.3 and 71.0 eV. This result indicated that a part of the platinum particles reduced by the heat-treatment

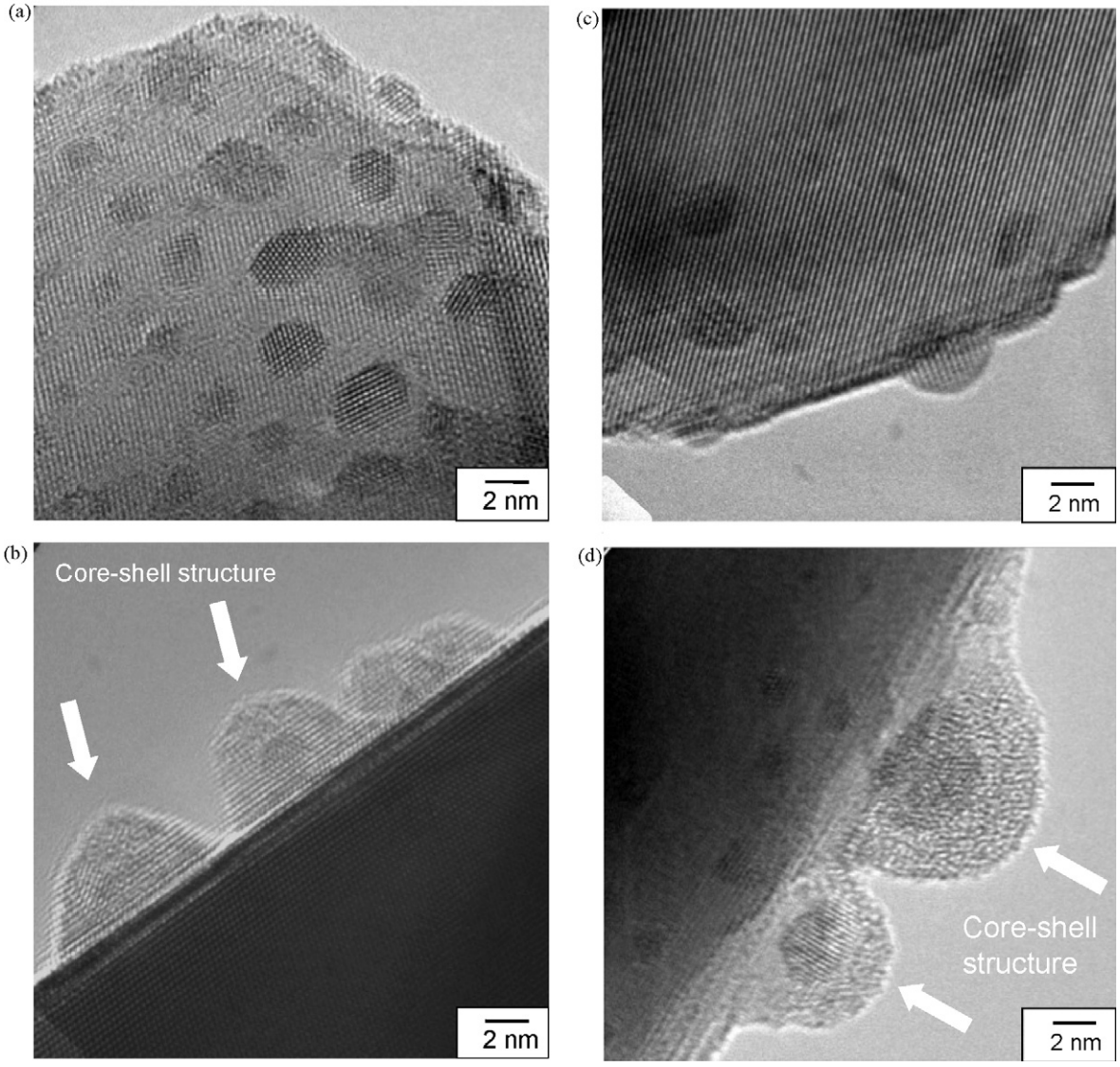


**Fig. 5.** FE-TEM images of 1.0 wt.% $Pt/SnO_2$ catalysts: (a) S-1, (b) S-2, (c) S-3, and (d) S-4.

in hydrogen was reoxidized to the Pt(IV) state by the reoxidation treatment at 400 °C. In other words, the platinum particles in the oxidation state and those in the metallic state existed in the reoxidized sample (S-3). Thereby, the recovery of catalytic activity after the reoxidation treatment in Fig. 2 will not be sufficient, though the treatment conditions (temperature, atmosphere, and time) of reoxidation were the same as those of calcination. In the case of the second reduced sample (S-4), the Pt 4f spectrum was similar to that of S-2. Thus, the platinum particles in reduced and second reduced samples were in the metallic state of Pt(0). In a comparison of the catalytic activities and the Pt 4f spectra, the oxidized platinum components gave rise to the high catalytic activity of ethyl acetate combustion. The difference in the peak positions was not detected in the Sn 3d spectra as can be seen in Fig. 4(b). However, the broad shoulder peaks around 484–486 eV were observed in the spectra of S-2 and S-4. Accordingly, a part of tin components on the surface of $SnO_2$ particles was slightly reduced, resulting in the formation of the intermetallic compounds analyzed by XRD.

Fig. 5 shows the FE-TEM images of 1.0 wt. % $Pt/SnO_2$ catalysts (S-1 ~ S-4). The fine particles with the diameter of *ca.* 2 nm were highly dispersed on the $SnO_2$ support in the as-calcined $Pt/SnO_2$ catalyst (Fig. 5(a)). Thus, the platinum species in S-1 were not detected by XRD apparatus in spite of the high loading amount of 10 wt.%. The lattice fringes were clearly observed in the regions of platinum deposits with the polygonal shapes, indicating that the platinum deposits were in well-crystallized state. After the $Pt/SnO_2$ catalyst was reduced in hydrogen, the distinctive particles with the core–shell structure were observed as can be seen in Fig. 5(b). The diameter of particles with the core–shell structure was *ca.* 5 nm, and was larger than that of the well-crystallized particles in S-1. In the case of the reoxidized sample (S-3), it is interesting that the fine particles with the size of *ca.* 2 nm were observed again (Fig. 5(c)), as in the case of S-1. Thereby, the deteriorated catalytic activity of S-2 was partially activated by the reoxidation treatment. In addition, the particles with the core–shell structure were formed after the second reduction treatment (Fig. 5(d)). The investigations on the core–shell structure have been reported so far [17,18]. In these studies, it was suggested that the core–shell structure was formed by the phase separation of tin species from the particles with the intermetallic compounds under a mild oxidative atmosphere, and the core and shell parts consisted of the intermetallic compounds and the amorphous $SnO_x$, respectively. Thus, in the formation process of the core–shell structure, the platinum species of the active site for catalytic reactions were encapsulated by $SnO_x$, resulting in the degradation of the catalytic activity. Moreover, the degradation will be attributed to the particle growth and the varieties of the surface electronic state due to the formation of the intermetallic compounds. From the TEM observation, it was confirmed the structural changes from the fine particles to the particles with the core–shell structure were reversible under the reduction–oxidation treatment. The changes in the morphology and the surface electronic state induced by the treatments will be related to the varieties of the catalytic activities. Consequently, the high catalytic activity of ethyl acetate combustion should originate from the exposed platinum particles with the oxidized state.

## 4. Conclusions

The catalytic activities for toluene combustion over the $SnO_2$-supported precious metal catalysts were investigated, and compared with the results of characterizations. From the experiments, it was concluded that the $Pt/SnO_2$ catalyst exhibited the highest activity due to the precious metal species in the high oxidation state. Subsequently, the catalytic activities for ethyl acetate oxidation over the $Pt/SnO_2$ catalyst treated under the redox atmosphere were studied in detail. The catalysts treated under the oxidative condition attained the high activity. Meanwhile, after the reduction treatment, the activities were deteriorated due to the particle growth, and the formation of the particles with intermetallic compounds and the core–shell structure. Additionally, it was confirmed that the changes in the morphology, surface electronic state, and catalytic activity were reversible corresponding to the reduction–oxidation treatments. The activation of deteriorated catalysts by oxidation treatment should play an important role in the effective use of the precious metal such as platinum.

## Acknowledgment

This work was supported by the Core Research for Evolutional Science and Technology (CREST) of Japan Science and Technology Agency (JST).

## References

[1] B.J. Finlayson-Pitts, J.N. Pitts Jr., Science 276 (1997) 1045.
[2] Z. Meng, D. Dabdub, J.H. Seinfeld, Science 277 (1997) 116.
[3] T.B. Ryerson, M. Trainer, J.S. Holloway, D.D. Parrish, L.G. Huey, D.T. Sueper, G.J. Frost, S.G. Donnelly, S. Schauffler, E.L. Atlas, W.C. Kuster, P.D. Goldan, G. Hübler, J.F. Meagher, F.C. Fehsenfeld, Science 292 (2001) 719.
[4] R. Atkinson, J. Arey, Chem. Rev. 103 (2003) 4605.
[5] J. Barbier Jr., L. Oliviero, B. Renard, D. Duprez, Catal. Today 75 (2002) 29.
[6] S. Hosokawa, H. Kanai, K. Utani, Y. Taniguchi, Y. Saito, S. Imamura, Appl. Catal. B: Environ. 45 (2003) 181.
[7] N. Li, C. Descorme, M. Besson, Appl. Catal. B: Environ. 71 (2007) 262.
[8] E.M. Cordi, J.L. Falconer, J. Catal. 162 (1996) 104.
[9] H. Widjaja, K. Sekizawa, K. Eguchi, Chem. Lett. 6 (1998) 481.
[10] H. Widjaja, K. Sekizawa, K. Eguchi, Bull. Chem. Soc. Jpn. 72 (1999) 313.
[11] K. Sekizawa, H. Widjaja, S. Maeda, Y. Ozawa, K. Eguchi, Appl. Catal. A: Gen. 200 (2000) 211.
[12] T. Takeguchi, O. Takeoh, S. Aoyama, J. Ueda, R. Kikuchi, K. Eguchi, Appl. Catal. A: Gen. 252 (2003) 205.
[13] T. Mitsui, K. Tsutsui, T. Matsui, R. Kikuchi, K. Eguchi, Appl. Catal. B: Environ. 81 (2008) 56.
[14] T. Matsui, T. Okanishi, K. Fujiwara, K. Tsutsui, R. Kikuchi, T. Takeguchi, K. Eguchi, Sci. Technol. Adv. Mater. 7 (2006) 524.
[15] T. Okanishi, T. Matsui, T. Takeguchi, R. Kikuchi, K. Eguchi, Appl. Catal. A: Gen. 298 (2006) 181.
[16] T. Matsui, K. Fujiwara, T. Okanishi, R. Kikuchi, T. Takeguchi, K. Eguchi, J. Power Sources 155 (2006) 152.
[17] N. Kamiuchi, T. Matsui, R. Kikuchi, K. Eguchi, J. Phys. Chem. C 111 (2007) 16470.
[18] N. Kamiuchi, K. Taguchi, T. Matsui, R. Kikuchi, K. Eguchi, Appl. Catal. B: Environ. 89 (2009) 65.
[19] N. Kamiuchi, T. Mitsui, H. Muroyama, T. Matsui, R. Kikuchi, K. Eguchi, Appl. Catal. B: Environ., in press.
[20] T. Mitsui, K. Tsutsui, T. Matsui, R. Kikuchi, K. Eguchi, Appl. Catal. B: Environ. 78 (2008) 158.